Computational Materials Science 153 (2018) 88–96

Contents lists available at ScienceDirect

Computational Materials Science

journal homepage: www.elsevier.com/locate/commatsci

Thermoelectric effect in superlattices; applicability of coherent and incoherent transport models

Lars Musland[a], Espen Flage-Larsen[b,c,*]

[a] University of Oslo, Department of Physics, P.O. Box 1048 Blindern, NO-0316 Oslo, Norway
[b] SINTEF Industry, Material Physics, P.O. Box 124 Blinder, NO-0314 Oslo, Norway
[c] University of Stavanger, Department of Mechanical and Structural Engineering and Materials Science, Ullandhaug, NO-4036 Stavanger, Norway

ARTICLE INFO

Keywords:
Electron transport
Thermal transport
Landauer
Buttiker approximation
Heterestructure
Superlattice

ABSTRACT

Calculations of thermoelectric transport coefficients including quantum effects are performed on superlattices using the Buttiker approximation. The results are compared to the Boltzmann transport equation with minibands present, and to an incoherent transport model. Comparisons are performed in the linear regime for the electrical conductivity, Seebeck and Lorenz coefficients. We show that at superlattice periods smaller than the typical electron mean free path, the former model and the calculations including quantum effects are in agreement. However, for longer superlattices the incoherent model is shown to be more correct.

1. Introduction

The thermoelectric properties are often improved by nano structuring [1] materials. This improvement stems mostly from a reduction of the thermal conductivity due to a reduced phonon mean free path. However, such modifications could also have a positive impact on the transport of charge carriers. Inclusion of nanoscale structures affects both the electronic structure and the scattering properties of carriers, and if tailored properly, these effects could increase the thermoelectric conversion efficiency.

An approach to nanostructuring that is motivated by this, is the concept of energy filtering [2–6]. In this approach the contributions to the electrical conductivity at different carrier energies are modified [7,3]. These contributions are contained in what is usually referred to as the transport distribution function. For applications of thermoelectricity, it is beneficial that the transport distribution function is asymmetric and sharply peaked close to the chemical potential. Previously it has been shown that the ideal shape of the transport distribution function is a delta function [7,8]. Unfortunately this can never be achieved, but by utilizing the flexibility of nano structuring it might be possible to approach this ideal case.

The concept of energy filtering rely on the possibility to tune the alignment of the charge carrier energy levels between different layers of materials. A model system where such effects can be studied is for instance periodic heterostructures, also known as superlattices. Consequentially, an extensive literature has appeared that address how the thermoelectric effect behaves in superlattices. Some of these suggest there is a large potential for improving the conversion efficiency by this approach [9–12,3]. Apart from isolated cases [13,14], experimental demonstration of such improvement is largely absent. This discrepancy could have several different sources. In fact, the synthesis and measurement phases are inherently difficult. However, it has also been suggested that the discrepancies between experiment and theory are mainly due to the approximations employed in the applied theoretical models [15].

Thus, there is a need too investigate less approximate models. For this purpose, several considerations are important. It might be necessary to: (i) include multiple bands past the effective mass approximation. (ii) include electrostatic interactions due to charge redistribution, as well as strain effects in the heterostructure. (iii) explicitly consider both the correct atomistic structure of the superlattice that is targeted, and also how close the synthesis process actually gets to that ideal case: Both interface roughness and deviations from the ideal periodic structure should be accounted for in the model. (iv) use better models for the carrier scattering. This applies in particular to the constant relaxation time approximation which is often employed. In order for the model to have predictive power, scattering models should either be developed from ab initio, or be based on empirical models that have been rigorously demonstrated to hold in a large number of different heterostructures. And finally, (v) consider the validity of the applied transport formalism.

The latter topic will be the subject of this work. The transport formalism that is usually applied to bulk thermoelectric materials is the semiclassical Boltzmann transport equation (BTE) [16–19]. Commonly,

* Corresponding author at: SINTEF Industry, Material Physics, P.O. Box 124 Blinder, NO-0314 Oslo, Norway.
E-mail address: espen.flage-larsen@sintef.no (E. Flage-Larsen).

https://doi.org/10.1016/j.commatsci.2018.05.044
Received 4 January 2018; Received in revised form 2 May 2018; Accepted 21 May 2018
Available online 26 June 2018

the BTE is linearized and used within the relaxation time approximation (RTA), thus making calculations particularly tractable [18]. The BTE is also applied to heterostructures.

However, it is not clear how the heterostructural properties of a superlattice should be treated in the BTE. One possibility is to assume a position dependent charge carrier energy dispersion relation upon solving the BTE itself. However, according to the uncertainty principle a position dependent dispersion relation is ill defined at the nanoscale. Another possibility is to use the band structure of the dominant material, and to treat the interfaces and barriers as a scattering mechanism. This approach has been pursued utilizing tractable, but not necessarily realistic models of interface scattering [10,20–23]. It is also possible to use the BTE within individual layers of the heterostructure, and treat transport of carriers between layers as an instance of thermionic emission [24,11,25,26]. Finally, in the case of superlattices, the periodicity of the structure allow to apply Bloch's theorem to the heterostructure itself. The effect of heterostructuring is then included in the band structure [27–31,2,32–34]. Since the energy bands of the bulk material are split into smaller subbands known as minibands, this model has been referred to as the miniband transport model [35]. The miniband transport model also has a limited regime of validity [35].

Recently the thermoelectric effect in superlattices have been studied by the application of non-equilibrium Green's functions (NEGF) [36–44,15,45–52]. The advantage of NEGF, is that it is derived directly from quantum mechanics and does not rely on a semi-classical model like the variety of BTE that is usually applied. Information dependent on position can thus be included in the calculations without violating the uncertainty principle. Due to its computationally demanding nature, applications of NEGF to thermoelectric materials usually rely on the effective mass approximation and simplified scattering models. NEGF has however been applied beyond these approximations [53–56] in other fields, but usually only to ordered structures. Recently new techniques has appeared to tackle also disordered structures, typically by employing non-equilibrium coherent potential approximation (NECPA) [57,58].

Studies of the range of validity of the BTE and the NEGF approach are thus of great interest. For the case of superlattices, Wacker [35,59–61] have made a significant contribution. In particular Wacker concludes that the miniband transport model is in agreement with NEGF when the superlattice wells are strongly coupled in comparison both to the scattering rate and to the electric field. Furthermore, he describes two other approximate schemes, valid when the scattering rate or the electric field is strong, respectively. These approximate models are justified in three different ways: by heuristic arguments, by formal derivation from NEGF, and finally by direct comparison of numerical calculations. Thus, Wacker demonstrates quite thoroughly the existence of three regimes where approximations to the NEGF formalism are valid.

However, Wacker's work was exclusively concerned with electrical conductivity σ. For thermoelectric applications, the Seebeck coefficient α [17,18] and the Lorenz coefficient L [62,63] are equally important. In addition, Wacker was mostly concerned with transport at high fields. In thermoelectric applications we are mostly concerned with low fields, or linear transport. A comparison of this kind was made in one recent work employing NEGF [37]. However, this work was limited to heterostructures with a total spatial extent of 6 nm. Since the bulk BTE expressions only apply in the diffusive regime, the sample should be considerably thicker in order for the results to be comparable.

The purpose of this study is to extend the work of Wacker to include also the Seebeck and Lorenz coefficient at low field for superlattices with different thickness. This work is not about obtaining experimental accuracy or reproducibility, but to investigate how quantum effects modify the themoelectric transport coefficient and how these results differ from the results from the BTE.

In this work we consider the most important quantum effects to include to be the wave nature of carriers, and the momentum and coherence loss caused by scattering. Accordingly, we have chosen to use a ballistic quantum transport simulator, which inherently captures the wave nature of carriers, and to incorporate the effects of momentum and coherence loss by the use of Buttiker probes [64,65,54,49–52,39,36]. The Buttiker probes are a set of virtual floating contacts attached to the ballistic system. Since these probes are floating, their only effect on the system is to randomize the momentum and phase of the carriers similar to a scattering mechanism. This approach is often referred to as the Buttiker approximation [36]. It is related to NEGF, but is less general and usually bears a lower computational cost. The Buttiker probes are described by self energies, in the same way as scattering processes are in NEGF. However, a key difference between the two methods is that the Buttiker approximation does not allow for the explicit definition of lesser self energies [64,66]. In practice this yields less control of the assignation of new states to carriers after scattering [64].

This work is organized as follows: The theoretical aspects are described and discussed in Section 2, where our quantum transport approach is described in Section 2.1. Sections 2.2 and 2.3 describes respectively the miniband transport model, and a second semiclassical approach that assumes incoherent transport between barriers. In Section 3 we show the results of our calculations. There we make two separate studies where we compare the electrical conductivity, the Seebeck and the Lorenz coefficient, as calculated by the Buttiker approximation, the miniband transport model, and by the incoherent model of Section 2.3. In Section 3.1 we study how the agreement between the models depend on the scattering rate, while in Section 3.2 we study how this agreement is affected by the size of the superlattice period. Finally, in Section 4 we provide final discussion and conclusions.

2. Theory and models

2.1. The Buttiker approximation

We utilize a ballistic quantum transport simulator with Buttiker probes [64,65]. The employed simulator is Kwant [67,68], which requires the definition of a tight binding model in the transport region, and a set of attached leads. Kwant efficiently solves the resulting quantum mechanical scattering problem, using either a wave function or a Green's function based approach. On completion, the ballistic transmission functions between the leads are obtained.

Only two of the leads attached to the transport region represent real contacts. These are the emitter and collector, between which currents would be measured in an experiment. The remaining leads are Buttiker probes, which are included to emulate scattering processes. For reasons of computational efficiency, the Buttiker probes are only connected to a subset of the sites in the transport region, and the density of Buttiker probes are controlled by the parameter d_{sc}. More specifically, the Buttiker probes are attached at regular intervals between the two real contacts, with one single probe per d_{sc} unit cells of the materials composing the heterostructure.

The interactions between the leads and the scattering region are described by retarded self energy functions [64,68]. In this work, the retarded self energies of the Buttiker probes are defined as $\Sigma^r = -i\hbar/2\tau$, which result in the relaxation of carrier momentum with a characteristic relaxation time τ [69,50]. This allows for a particularly simple comparison to the BTE within the RTA. When $d_{sc} > 1$, the scattering self energies are modified to $\Sigma^r = -d_{sc} \cdot i\hbar/2\tau$, to compensate for the lower density of Buttiker probes. The magnitude of the self energies of the contacts are not of significance, since our calculations are made in such a way as to be independent of contact effects. Please consult our previous work for additional details [69].

The retarded self energy functions describe how carriers are absorbed by the Buttiker probes [64]. In addition, it is necessary to describe how carriers are emitted. Within the NEGF formalism, carriers

that enter the system are described by the lesser self energies $\Sigma^<$ [64]. However, within our ballistic framework, these cannot be explicitly defined. Instead, we define the re-emission of carriers after absorption by a Buttiker probe as follows: Carriers are re-emitted from the same probe at which they were absorbed with the same energy and momentum orthogonal to the transport direction as before absorption. The momentum component parallel to the transport direction is randomized. The scattering process thus conserves charge, energy and transverse momentum. The conservation of energy is by choice, since we want to model elastic scattering. On the other hand, the conservation of transverse momentum is only introduced for reasons of computational efficiency.

By extending the expression for transmission [64,69], we use Kwant together with the scheme described earlier to calculate the effective transmission between the two real contacts. Since only elastic scattering is present, we make use of the Landauer transport formalism to connect the effective transmission function to the relevant transport coefficients. These are in our case the electrical conductivity σ, the Seebeck coefficient [17,18] α and the Lorenz coefficient L. The latter is defined as $\kappa_e = \sigma L T$ [62,63]. Here κ_e is the electron contribution to the thermal conductivity. In the linear regime, the magnitude of these coefficients in the cross plane direction can be expressed as [69–71]

$$\sigma = \int \mathrm{d}E\, \Sigma(E) F_T(E), \tag{1a}$$

$$\alpha = -\frac{1}{\sigma e T} \int \mathrm{d}E\, \Sigma(E) F_T(E)(E-\mu), \tag{1b}$$

$$L = \frac{1}{\sigma e^2 T^2} \int \mathrm{d}E\, \Sigma(E) F_T(E)(E-\mu)^2 - \alpha^2. \tag{1c}$$

where $\Sigma(E)$ is the transport distribution function, and $F_T(E)$ is the thermal broadening function or Fermi window $F_T(E) = -\partial f/\partial E$, where f is the Fermi-function.

2.2. The miniband transport model

Following Wacker's nomenclature [35], we refer to the application of the BTE, using the band structure of the superlattice, as the miniband transport model. The superlattice band structure may be obtained by schemes of varying approximation, ranging from the introductory Kronig Penney model [27,28,72] to ab initio approaches such as DFT [30,34]. In this study we use the band structure resulting from the solutions of the same tight binding model used in the Kwant simulations discussed above as input to the BTE. This allows for a direct comparison of the results, without considering differences in electronic structure between the models. In addition, the tight binding model allows calculations on superlattices with very large periods with acceptable accuracy.

The validity of the miniband transport model have been extensively investigated by Wacker [35,59]. He describes two conditions $t \gg \hbar\Gamma$ and $t \gg eFa$, both of which must be satisfied for the miniband model to be valid. Here t is the coupling energy between neighboring wells of the superlattice, Γ is the scattering rate, F is the applied electric field, and a is the superlattice period. In this work we study linear transport and the latter condition is satisfied by definition. The former may be heuristically rewritten as follows: within a simple nearest neighbor tight binding description, the miniband energy dispersion along the growth direction is given by $E(k) = 2t\cos ka$. Thus, the velocity is $v = \partial E_k/\partial k/\hbar \sim ta/\hbar$. Given this, we may rewrite Wacker's first condition as

$$a \ll v\tau. \tag{2}$$

Here $\tau = 1/\Gamma$ is the average scattering time, which in the case of our simple scattering model is equal to the momentum relaxation time. In our previous work [69], Eq. (2) was also derived by a heuristic argument involving Heisenberg's uncertainty relations.

The product $v\tau$ will generally be similar to the coherence length [64] l_ϕ. As such Eq. (2) is thus equivalent to a condition stated in previous work [10,2], namely that the superlattice period should be shorter than l_ϕ for the miniband model to apply. This condition is intuitive, since the minibands always arise from the solution of some wave equation. When $a > l_\phi$, the electron behavior is not coherent within the unit cell, and accordingly no wave equation is applicable.

2.3. The sequential transmission model

In addition to the case $t \gg \hbar\Gamma$, Wacker also describes an approximate model that applies in the opposite limit $t \ll \hbar\Gamma$ [35,59], here given by $a \gg v\tau$. This model, which he refers to as the sequential tunneling model, is extensive and involves scattering theory beyond Fermi's golden rule. The reason why this is necessary, is that the applied field misaligns the energy levels of the different wells, so that first order scattering expressions result in zero current due to energy conservation [35]. However, since we here only study linear transport, we express the currents in terms of transmission functions at zero bias [64], where this does not pose a problem.

Thus, we make use of another model employed in previous work [20], which we will refer to as the sequential transmission model. It is derived here again for consistency. A central assumption for proceeding is that transport between different wells in the superlattice is incoherent [35]. We then use incoherent transmission functions [73] in series, expressed as

$$\frac{1}{T} = \frac{1}{T_1} + \frac{1}{T_2} - 1. \tag{3}$$

The transmission through a single superlattice period can be found from this by substituting the well transmission T_w for T_1, and the barrier transmission T_b for T_2. The transmission through N periods can then be found by applying the addition formula inductively to get

$$\begin{aligned} \frac{1}{T} - 1 &= N\left(\frac{1}{T_w} + \frac{1}{T_b} - 2\right) \\ &= N\left(\frac{1}{T_w} - 1\right) + \frac{L}{a}\left(\frac{1}{T_b} - 1\right), \end{aligned} \tag{4}$$

where L is the total length of the N periods.

In the case where there are no barriers present we obtain by the same procedure

$$\frac{1}{T_{bulk}} - 1 = N\left(\frac{1}{T'_w} - 1\right), \tag{5}$$

where T'_w is the transmission function of the well sections. Since these sections are thicker in absence of barriers, $T'_w \neq T_w$. However, if the well sections are considerably thicker than the barriers, then the change in thickness will be small and $T_w = T'_w$ is a good approximation. In this case, we may combine Eqs. (4) and (5) such that

$$\frac{1}{T} - 1 = \frac{1}{T_{bulk}} - 1 + \frac{L}{a}\left(\frac{1}{T_b} - 1\right). \tag{6}$$

In the literature, we also find the back scattering mean free path λ defined through the expression $1/T - 1 = L/\lambda$ [73,70]. Inserting this, Eq. (6) becomes

$$\frac{1}{\lambda} = \frac{1}{\lambda_{bulk}} + \frac{1}{a}\left(\frac{1}{T_b} - 1\right), \tag{7}$$

which applies in the limit where both $a \gg v\tau$ and $a \gg b$, with b being the thickness of the barriers. If we also assume $b \ll v\tau$, we can approximate T_b to be ballistic, which allows for more efficient calculations.

Within the Landauer transport formalism, the transport distribution function $\Sigma(E)$ is determined by the back scattering mean free path [70] and Eq. (7) is thus sufficient to determine the thermoelectric transport

coefficients σ, α and L. One can also use the derived expressions for the transport in the Landauer approach and the BTE [70,69] to express Eq. (7) in terms of relaxation times in the RTA. The resulting expression becomes

$$\frac{1}{\tau} = \frac{1}{\tau_{bulk}} + \frac{2v}{a}\left(\frac{1}{T_b} - 1\right), \tag{8}$$

and must be used in the BTE together with the band structure of the well material. This expression is an instance of Matthiessen's rule [66]: The first term on the right is the relaxation rate of the bulk well material, while the last term is the relaxation rate of scattering on barriers.

3. Results

The transport distribution function is calculated from the transmission function [64] by utilizing the Landauer formalism. Please consult our previous work [69], where this approach is explained in detail. Additional details can also be found in the literature [73,64,70,71]. In this work we again utilize CdTe and CdHgTe alloys as a model system. Their only role of this work is to provide a somewhat realistic system from which the band structure can be constructed. Details of the tight-binding model and fitting procedure from first-principle calculations, as well as the resulting parameters, can be found in our previous work [69].

3.1. Dependence on the scattering time.

According to the discussion of Section 2.2 we expect agreement between the Buttiker and the miniband model for large values of τ. At smaller values this agreement should disappear, and the quantum transport model should eventually agree with an incoherent model. In this section, the calculations are performed on a superlattice containing at total of 16 unit cells, eight of CdTe followed by eight of $Cd_{0.75}Hg_{0.25}Te$. The resulting spectral function and transport properties are shown in Fig. 1 for different values of τ, ranging from 1 fs to 0.1 ps. At larger values of τ, the thickness L of the simulated region must be larger in order for the transport process to remain incoherent. Accordingly, L is chosen respectively as 337, 169, 84.5 and 42.3 nm for $\tau = 100$, 50, 20 and 10 fs, and as 21.1 nm (two superlattice periods) for $\tau = 5$, 2 and 1 fs. Similarly, at smaller values of τ the coherence length is shorter, so that d_{sc} must be smaller in order to sample structures at smaller length scales. Thus, we choose $d_{sc} = 2$ when $\tau = 100$, 50 or 20 fs, and $d_{sc} = 1$ when $\tau = 10$, 5, 2 or 1 fs.

The operating principles behind these choices are that we always have $L \gtrsim 4v\tau$, while d_{sc} satisfies both $d_{sc} \leqslant 2$ and $d_{sc}a < v\tau/4$. The first two of these conditions originate from our previous work [69], while the latter is a heuristic condition based on the desire to have a reasonable sampling of the coherence length. The group velocity v is estimated to $\hbar\langle v\rangle = \langle \partial E/\partial \boldsymbol{k}\rangle \approx 0.6$ eVÅ, from the band structure of the $Cd_{0.75}Hg_{0.25}Te$ model [69].

Our implementation of the Buttiker approximation calculates the transport distribution function as an integral over the transverse component of k-space. This integration makes use of the midpoint method, and is performed in cylindrical coordinates. The integration grid has an evenly distributes sampling of $N_k = 100$ points in the radial $\boldsymbol{k}$-direction, and a distance of $\delta_\theta = 0.03$ between points in the angular direction in direct $\boldsymbol{k}$-space [69]. Calculation of transport coefficients requires integration over energy, which also utilize the midpoint method on a regular sampling of $N_E = 200$ points between $E_{min} = 2.0$ eV and $E_{max} = 4.0$ eV. This interval surrounds the band gaps of the involved materials, as can be seen in our previous work [69].

The routines to perform the BTE calculations required by the miniband transport model, are explained in detail in a separate work [74]. In summary a regular cubic integration grid was used, employing a resolution of $N_k^{xy} = 51$ points in the k_x and k_y directions, and $N_k^z = 13$ points in the k_z direction, which is the transport direction and the cross plane direction of the super lattice. These choices were again based on convergence studies performed in our previous work [69]. The tight binding model was used to generate the band structure on this grid followed by a step of numerical differences to extract the velocities. Finally, a trapezoidal integration scheme was performed. The relaxation time was fixated at 1 fs to be compatible with the model used for the Buttiker model.

In Fig. 1a, we present the results of $\Sigma(E)/\tau$ for different values of τ. Since evaluating $\Sigma(E)$ using the BTE is demanding, we show only results of the Buttiker approximation and the sequential transmission model. However, in our previous work we demonstrated that our implementation of the Buttiker approximation is in agreement with the miniband transport model for short period superlattices and large values of τ, in agreement with Section 2.2. We thus expect the miniband transport result to largely agree with results from the Buttiker approximation at $\tau = 100$ fs. Since the BTE expression for $\Sigma(E)$ is proportional to τ [18,17], the miniband results with smaller values of τ would also be identical to this curve. The calculated results from the miniband model contains numerical noise, which originates from a too course integration grid. As we approach a very low temperature which is required to produce $\Sigma(E)$ an extremely dense integration grid is needed. In the calculation of transport coefficients, this noise is smeared by the finite temperature, and is thus not of particular significance. In order not to confuse readers we thus opted not to show these results in Fig. 1a.

The sequential transmission model does not agree with the Buttiker approximation, even for small values of τ. However, such agreement is not to be expected here. In addition to the requirement $v\tau \ll a$, $a \gg b$ also need to be satisfied. This is not the case, since $b = a/2 = 5.3$ nm. The sequential transmission model is by design more suited for large superlattice periods than small values of τ. Small values of τ may instead require a more sophisticated sequential model, such as the one described by Wacker [35,59].

Figs. 1b–d compare the electrical conductivity, Seebeck and Lorenz coefficients calculated using the Buttiker approximation and the miniband transport model. The sequential transmission model is not shown, since its failure is demonstrated already in Fig. 1a. In Fig. 1b the electrical conductivities are normalized by the magnitude of τ. This makes the miniband transport results independent of τ in all three figures, due to the cancellation of a constant relaxation time in the α and L [18,17]. The miniband transport results are in good agreement with those of the Buttiker approximation when $\tau = 100$ fs, but when τ is reduced the agreement gradually disappears. This effect is in agreement with the discussion concerning Eq. (2).

In all four Figs. 1a-d, we see clear oscillations in the transport coefficients as a function of the chemical potential μ. This effect originates when the chemical potential is varied, and the contributions from the minibands are picked up. When τ is decreased, the oscillations are gradually smeared, indicating that the miniband structure disappears. For the smallest values of τ, even variation in transport properties originating in the bulk band gap is beginning to smooth out. However, the disappearance of the band gap is probably an artifact of the crudeness of our scattering model. One can show that a scattering model of the type described in Section 2.1 will cause a Lorenzian broadening of eigenstates [64], which given sufficiently small values of τ will smooth out any structures in the transport properties. However, in the more realistic case of a non-constant relaxation time, the broadening of eigenstates can have a more complicated shape [64], allowing for the band gap to be maintained.

3.2. Dependence on the superlattice period

The question of dependence on the superlattice period is experimentally relevant to a larger extent than that of the previous section, since the scattering time tends to fall in the range τ=10–1000 fs, while

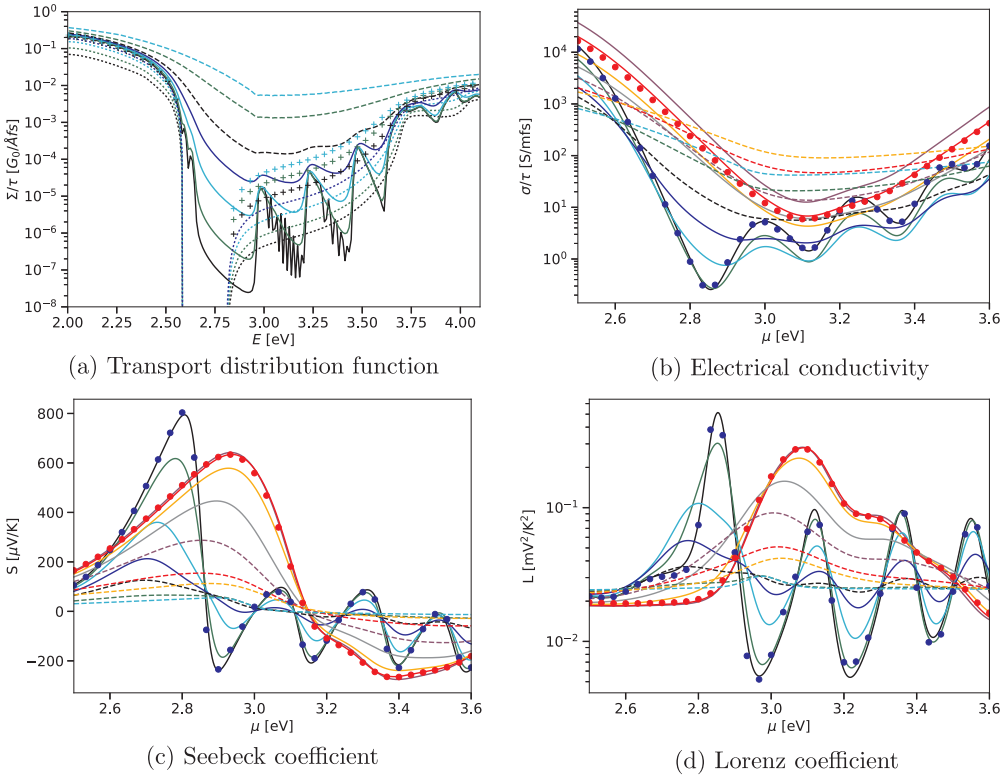

Fig. 1. Transport coefficients for electrons in an 8-8 CdTe-$Hg^{0.25}Cd^{0.75}Te$ superlattice as function of the chemical potential μ. The solid and dashed lines are calculated by the Buttiker approximation, the circles by the miniband transport model, and the dotted lines and crosses by the sequential transmission model. For the solid and doted lines, the black, green, turquoise and blue results are from calculations with τ = 100, 50, 20 and 10 fs, respectively. For the dashed lines and the crosses, the black, green and turquoise lines are from calculations with τ = 5, 2 and 1 fs, respectively. Furthermore, in panel (b–d) results in black, green, turquoise and blue are calculated at 300 K, while the purple, red, orange and gray lines are calculated at 700 K. Among the solid and dashed lines, the purple, red, orange and gray lines respectively have τ = 100, 50, 20 and 10 fs. Among the dashed lines and crosses the purple, red and orange lines have τ = 5, 2 and 1 fs respectively. The miniband results are shown as blue and red dots at 300 K and 700 K, respectively. (For interpretation of the references to colour in this figure legend, the reader is referred to the web version of this article.)

the superlattice period can be tailored during synthesis.

In Figs. 2 and 3, results are shown for several different superlattices, having periods ranging from 11 to 340 nm. All of the supercells are composed of a single barrier layer composed of eight unit cells of CdTe, and a single well layer composed of $Cd^{0.75}Hg^{0.25}Te$. The results from the Buttiker approximation were obtained at τ = 100 fs, with d_{sc} = 2,

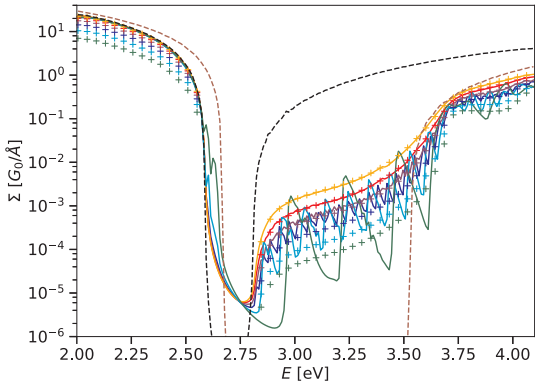

Fig. 2. Transport distribution function in multiple superlattices. Results shown in green, turquoise, blue, purple red and orange are calculated respectively with superlattice periods of 16, 32, 64, 128, 256 and 512 unit cells of the composing materials. Among these, solid lines represent the Buttiker approximation, while crosses represent the sequential transmission model. The brown and black dashed lines are respectively the transport distribution function of bulk CdTe and $Cd^{0.75}Hg^{0.25}Te$. (For interpretation of the references to colour in this figure legend, the reader is referred to the web version of this article.)

and using the same integration grid as in the previous section. The BTE calculations also use the same integration grid as in the previous section.

Fig. 2 shows the transport distribution function, which is compared to that of pure CdTe and $Cd^{0.75}Hg^{0.25}Te$. Only results from the Buttiker approximation and the sequential transmission model are shown. Comparison to the miniband transport model is left for Fig. 3 where we show respectively the conductivities, Seebeck coefficients and Lorenz coefficients of the mentioned superlattices, calculated at 300 and 700 K. Fig. 3 includes results from the Buttiker approximation, the sequential transmission model, and the miniband transport model.

At short superlattice periods, the Buttiker approximation is in reasonable agreement with the miniband transport model, while for large superlattice periods it agrees more closely with the sequential transmission model. Consequently, the expectation that Eq. (7) is valid for large periods is confirmed, also for the Seebeck and Lorenz coefficient. The transition between the two regimes is better illustrated in Fig. 4, which shows the calculated transport coefficients as a function of the superlattice period a at the three values of μ = 2.6, 3.0 and 3.35 eV. These chemical potentials are also illustrated by vertical lines in Fig. 3.

In all results where significant difference can be seen between the models, the Buttiker approximation changes from agreeing with the miniband model to the sequential transmission model at around a = 100 nm. As discussed above, the average group velocity of $Cd^{0.75}Hg^{0.25}Te$ in the conduction band is approximately 0.6 eVÅ. Since τ = 100 fs, $\langle v\rangle\tau \approx$ 90 nm. The transition at $a \sim$ 100 nm is thus confirmed to be close to the relaxation length $v\tau$, which gives confidence that the mean free path is a reasonable estimate of the transition point between the two regimes. In fact, within the accuracy to which this can be

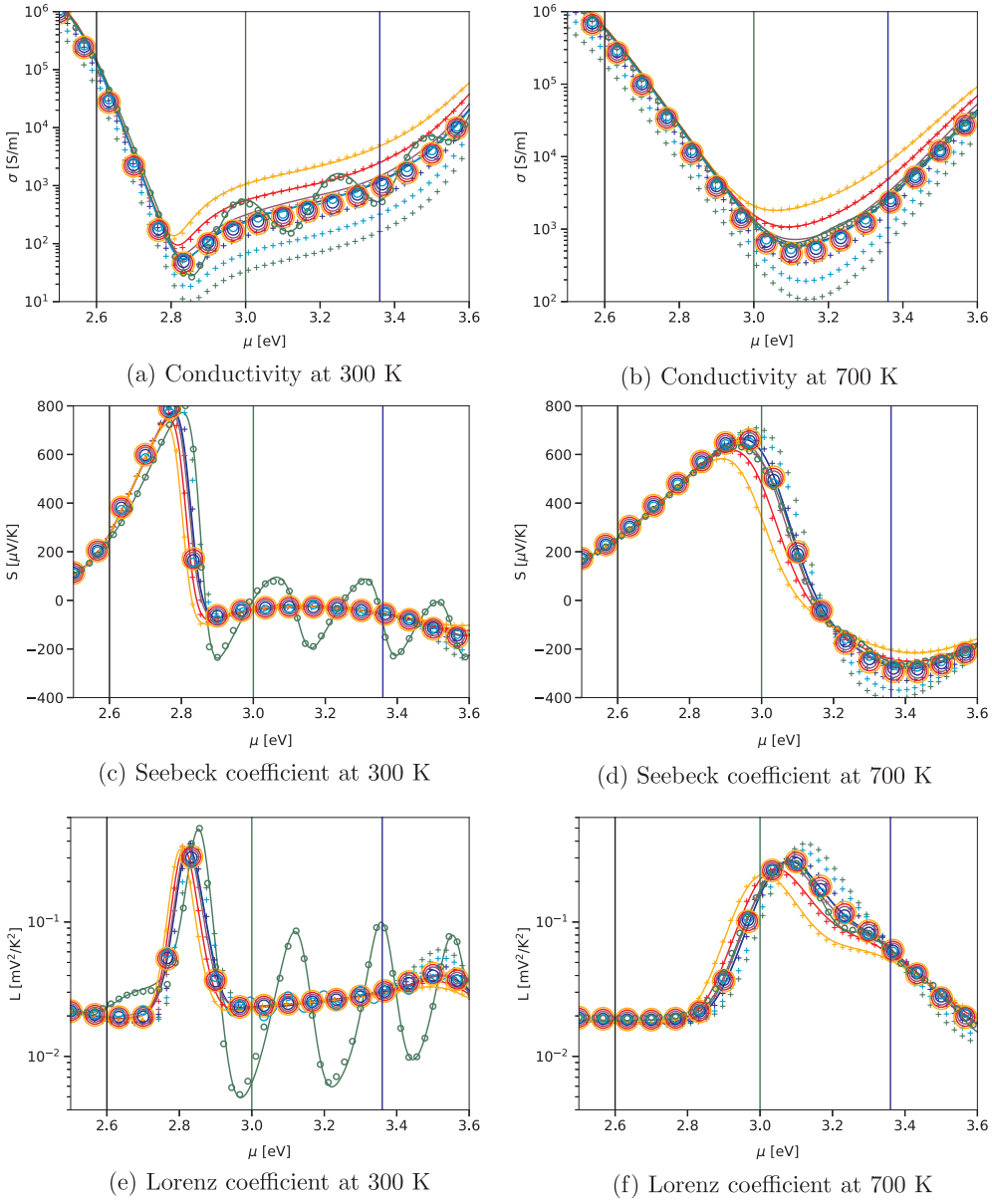

(a) Conductivity at 300 K (b) Conductivity at 700 K

(c) Seebeck coefficient at 300 K (d) Seebeck coefficient at 700 K

(e) Lorenz coefficient at 300 K (f) Lorenz coefficient at 700 K

Fig. 3. Transport coefficients in multiple superlattices as function of the chemical potential μ of electrons. Results shown in green, turquoise, blue, purple red and orange are calculated respectively with superlattice periods of 16, 32, 64, 128, 256 and 512 unit cells of the composing materials. Solid lines represent the Buttiker approximation, crosses represent the sequential transmission model, while circles represent the miniband transport model. The three vertical lines represent values of μ at which the dependence on period is examined more closely in Fig. 4. (For interpretation of the references to colour in this figure legend, the reader is referred to the web version of this article.)

judged, the transition seems to happen exactly at $a = v\tau$. However, this is likely to be an artifact of our simplified scattering model, where the momentum relaxation time is by construction equal to the coherence time [69]. In general we should expect the transition to happen near the phase relaxation length, of which the momentum relaxation length $v\tau$ is usually only a rough estimate [64].

We would also like to emphasize that the transition region in Fig. 4 appears to be quite small. If this fact generalizes, then the respective conditions $v\tau \gg a$ and $v\tau \ll a$ of the miniband transport and sequential transmission regimes, can be modified to $v\tau \gtrsim a$ and $v\tau \lesssim a$. The thermoelectric effect in superlattices can thus possibly always be studied using semiclassical approaches, and that the only role of quantum transport is to determine the transition point between the coherent and incoherent regimes. In order to confirm this, further studies are needed, which include different material systems and more realistic scattering mechanisms.

4. Summary and conclusion

The purpose of this work was to provide demonstrations of validity regimes of semiclassical treatment of electron transport in superlattices, extend earlier work [35,59–61] to also include thermoelectric transport coefficients, and to perform an exclusive treatment of the linear regime. Our approach utilized the Buttiker approximation, and performed explicit comparisons between the resulting transport coefficients and two different semiclassical models described in Sections 2.2 and 2.3.

We showed that the miniband transport model is better fit to reproduce the results of the Buttiker approximation for large values of the scattering time τ. We also compared the results of the Buttiker approximation to the sequential transmission model, and in the case of the structure with a short period discussed in Section 3.1, we found a poor match for all values of τ. However, as we showed, this is expected. In Section 3.2, we showed that the miniband transport model and the

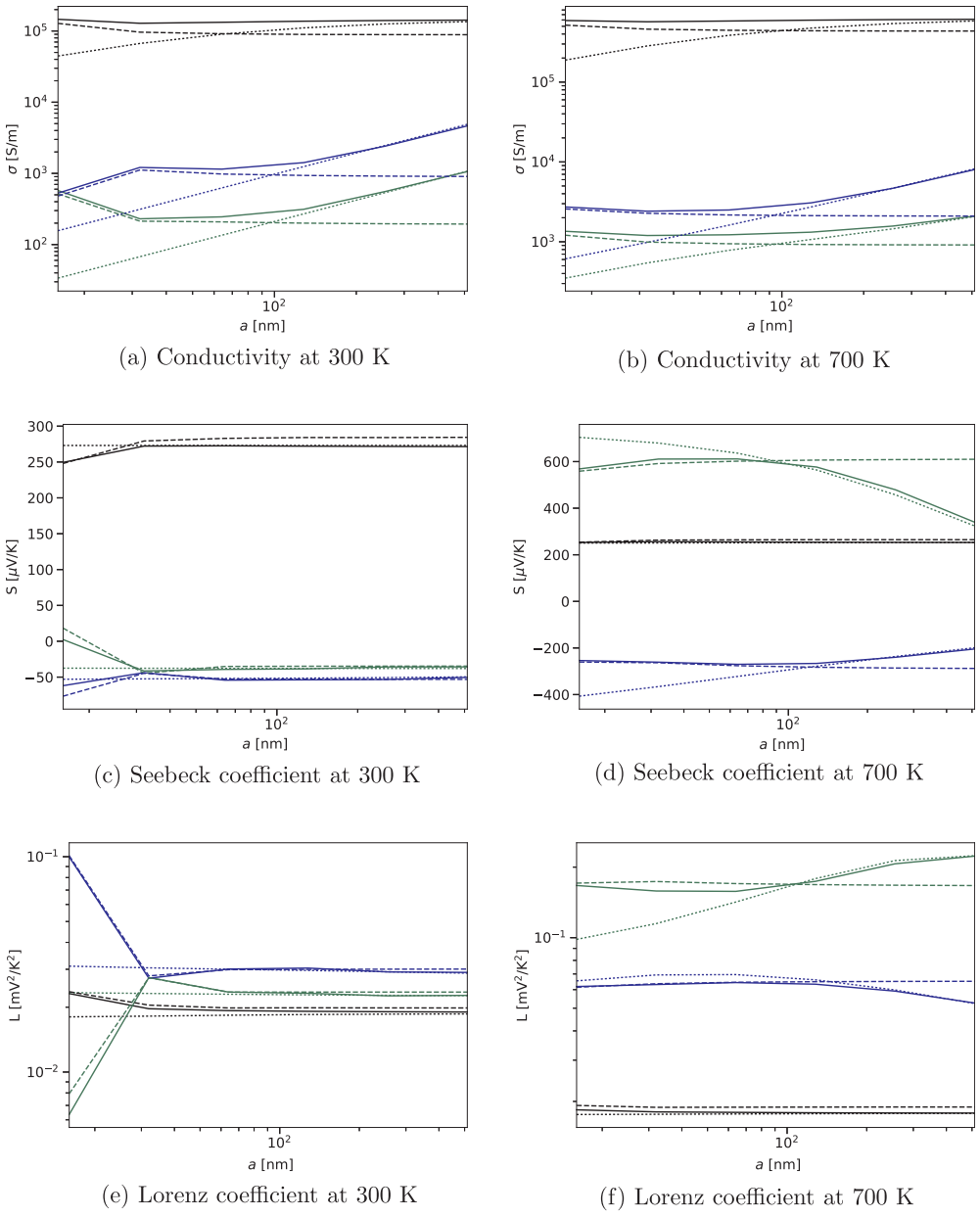

(a) Conductivity at 300 K (b) Conductivity at 700 K

(c) Seebeck coefficient at 300 K (d) Seebeck coefficient at 700 K

(e) Lorenz coefficient at 300 K (f) Lorenz coefficient at 700 K

Fig. 4. Transport coefficients as function of the superlattice period a. Results shown in black, green and blue are calculated respectively with a chemical potential of $\mu = 2.6$ eV, $\mu = 3.0$ eV and $\mu = 3.36$ eV. The different line styles represents different models. The solid lines represent the Buttiker approximation, the dashed lines the miniband transport model, while the dotted lines represent the sequential transmission model. (For interpretation of the references to colour in this figure legend, the reader is referred to the web version of this article.)

Buttiker approximation are in good agreement for superlattice periods shorter than ∼ 100 nm, while the sequential transmission model and Buttiker approximation are in agreement for periods larger than ∼ 100 nm. To summarize, our results are in excellent agreement with the expectations discussed in Sections 2.2 and 2.3, and with those stated in earlier works for the case of conductivity [35,59–61]. We can conclude that these observations should also hold for the Seebeck and Lorenz coefficient.

It has been argued that superlattices with high thermoelectric efficiency should have a short period to inhibit phonon transport [2]. Consequently they should then fall into the miniband regime which would simplify future interpretation and calculations significantly. However, a good thermoelectric material also requires a high electrical conductivity, which suggests that the superlattice period should be large, so as not to inhibit the motion of carriers. Increased focus on the electrical properties is also becoming increasingly important due to the fact that several bulk materials already possess a very low thermal conductivity below 1 W/m K. Secondly, there could be other ways of reducing phonon transport than having a short period. For instance, one could let the superlattice period itself have a complex structure. Accordingly, we conclude that the question of coherent versus incoherent transport models may in fact be important to the design of thermoelectric heterostructures, and that some special cases may even require a full quantum transport approach, such as the Buttiker approximation or NEGF.

Acknowledgments

We would like to acknowledge the Research Council of Norway (NANO2021 project Thelma, number 228854) for providing funding, and the Norwegian Metacenter for Computational Resources (NOTUR) for providing computational resources.

References

[1] E. Maciá, Thermoelectric Materials: Advance and Applications, Pan Stanford Publishing, 2015.
[2] Z. Bian, M. Zebarjadi, R. Singh, Y. Ezzahri, A. Shakouri, G. Zeng, J.-H. Bahk, J.E. Bowers, J.M.O. Zide, A.C. Gossard, Cross-plane Seebeck coefficient and Lorenz number in superlattices, Phys. Rev. B 76 (2007) 205311.
[3] E. Flage-Larsen, O.M. Løvvik, Materials, Preparation, and Characterization in Thermoelectrics, in: D.M. Rowe (Ed.), Band Structure Guidelines for Higher Figure-of-Merit: Analytic Band Generation and Energy Filtering, CRC Press, 2012 (Chapter 10).
[4] K. Berland, X. Song, P.A. Carvalho, C. Persson, T.G. Finstad, O.M. Løvvik, Enhancement of thermoelectric properties by energy filtering: theoretical potential and experimental reality in nanostructured ZnSb, J. Appl. Phys. 119 (12) (2016) 125103.
[5] D. Narducci, S. Frabboni, X. Zianni, Silicon de novo: energy filtering and enhanced thermoelectric performances of nanocrystalline silicon and silicon alloys, J. Mater. Chem. C 3 (47) (2015) 12176.
[6] X.H. Yang, X.Y. Qin, J. Zhang, D. Li, H.X. Xin, M. Liu, Enhanced thermopower and energy filtering effect from synergetic scattering at heterojunction potentials in the thermoelectric composites with semiconducting nanoinclusions, J. Alloy. Compd. 558 (2013) 203.
[7] Z. Fan, H.-Q. Wang, J.-C. Zheng, Searching for the best thermoelectrics through the optimization of transport distribution function, J. Appl. Phys. 109 (7) (2011) 073713.
[8] G.D. Mahan, J.O. Sofo, The best thermoelectric, Proc. Natl. Acad. Sci. USA 93 (1996) 7436–7439.
[9] L.D. Hicks, M.S. Dresselhaus, Effect of quantum-well structures on the thermoelectric figure of merit, Phys. Rev. B 47 (1993) 12727.
[10] L.W. Whitlow, T. Hirano, Superlattice applications to thermoelectricity, J. Appl. Phys. 78 (1995) 5460.
[11] G.D. Mahan, L.M. Woods, Multilayer thermionic refrigeration, Phys. Rev. Lett. 80 (1998) 4016.
[12] F. Zahid, R. Lake, Thermoelectric properties of Bi2Te3 atomic quintuple thin films, Appl. Phys. Lett 97 (21) (2010) 212102.
[13] R. Venkatasubramanian, E. Siivola, T. Colpitts, B. O'quinn, Thin-film thermoelectric devices with high room-temperature figures of merit, Nature 413 (6856) (2001) 597.
[14] J.M.O. Zide, D. Vashaee, Z.X. Bian, G. Zeng, J.E. Bowers, A. Shakouri, A. Gossard, Demonstration of electron filtering to increase the seebeck coefficient in In0.53Ga0.47 As/In0.53Ga 0.28Al 0.19 As superlattices, Phys. Rev. B 74 (20) (2006) 205335.
[15] M. Thesberg, M. Pourfath, N. Neophytou, H. Kosina, The fragility of thermoelectric power factor in cross-plane superlattices in the presence of nonidealities: a quantum transport simulation approach, J. Electron. Mater. 45 (3) (2016) 1584.
[16] A. Cantarero, F.X. Àlvarez, Nanoscale Thermoelectrics. Thermoelectric Effects: Semiclassical and Quantum Approaches from the Boltzmann Transport Equation, Springer International Publishing, Cham, 2014 Chapter 1.
[17] G. Grosso, G.P. Parravicini, Solid State Physics, Elsevier Science, 2013.
[18] N.W. Ashcroft, N.D. Mermin, Solid State Physics, Thomson Learning, 1976.
[19] G.K.H. Madsen, D.J. Singh, Boltztrap. A code for calculating band-structure dependent quantities, Comput. Phys. Commun. 175 (1) (2006) 67.
[20] A. Popescu, L.M. Woods, J. Martin, G.S. Nolas, Model of transport properties of thermoelectric nanocomposite materials, Phys. Rev. B 79 (20) (2009) 205302.
[21] C. Bera, M. Soulier, C. Navone, G. Roux, J. Simon, S. Volz, N. Mingo, Thermoelectric properties of nanostructured Si1- xGex and potential for further improvement, J. Appl. Phys. 108 (12) (2010) 124306.
[22] V. Brinzari, D.L. Nika, I. Damaskin, B.K. Cho, G. Korotcenkov, Thermoelectric properties of nano-granular indium-tin-oxide within modified electron filtering model with chemisorption-type potential barriers, Phys. E: Low-Dimen. Syst. Nanostruct. 81 (2016) 49–58.
[23] J.-H. Bahk, A. Shakouri, Minority carrier blocking to enhance the thermoelectric figure of merit in narrow-band-gap semiconductors, Phys. Rev. B 93 (16) (2016) 165209.
[24] A. Shakouri, J.E. Bowers, Heterostructure integrated thermionic coolers, Appl. Phys. Lett. 71 (9) (1997) 1234.
[25] D. Vashaee, A. Shakouri, Improved thermoelectric power factor in metal-based superlattices, Phys. Rev. Lett 92 (10) (2004) 106103.
[26] D. Vashaee, A. Shakouri, Electronic and thermoelectric transport in semiconductor and metallic superlattices, J. Appl. Phys. 95 (3) (2004) 1233–1245.
[27] Y.-M. Lin, M.S. Dresselhaus, Thermoelectric properties of superlattice nanowires, Phys. Rev. B 68 (7) (2003) 075304.
[28] D.A. Elhabti, P. Vasipoulos, J.F. Currie, Impact of impurities on superlattice transport-coefficients in the absence of a magnetic-field, Can. J. Phys. 69 (3-4) (1991) 465–473.
[29] G. Fiedler, L. Nausner, Y. Hu, P. Chen, A. Rastelli, P. Kratzer, Thermoelectric properties of Ge/Si heterostructures: a combined theoretical and experimental study, Phys. Stat. Solidi (a) 213 (3) (2015) 524.
[30] M. Salimi, S.J. Hashemifar, First-principles calculation of semiclassical thermoelectric properties of (agsbse 2) n (agsbte 2) n superlattices, J. Alloy. Compd. 650 (2015) 143.
[31] R.J. Radtke, H. Ehrenreich, C.H. Grein, Multilayer thermoelectric refrigeration in Hg1-xCdxTe superlattices, J. Appl. Phys. 86 (1999) 3195.
[32] J.-H. Bahk, R.B. Sadeghian, Z. Bian, A. Shakouri, Seebeck enhancement through miniband conduction in III–V semiconductor superlattices at low temperatures, J. Electron. Mater. 41 (2012) 1498.
[33] V.M. Fomin, P. Kratzer, Thermoelectric transport in periodic one-dimensional stacks of InAs/GaAs quantum dots, Phys. Rev. B 82 (2010) 045318.
[34] N. Hinsche, I. Mertig, P. Zahn, Lorenz function of Bi2Te3/Sb2Te3 superlattices, J. Electron. Mater. 42 (7) (2013) 1406.
[35] A. Wacker, Semiconductor superlattices: a model system for nonlinear transport, Phys. Rep. 357 (1) (2002) 1.
[36] T. Musho, Predicting the figure of merit of nanostructured thermoelectric materials, J. Mater. Res. 30 (17) (2015) 2628.
[37] A. Bulusu, D.G. Walker, Quantum modeling of thermoelectric properties of Si/Ge/Si superlattices, IEEE T. Electron Dev. 55 (1) (2008) 423.
[38] A. Bulusu, D.G. Walker, Modeling of thermoelectric properties of semi-conductor thin films with quantum and scattering effects, J. Heat Transf. 129 (4) (2007) 492.
[39] A. Bulusu, D.G. Walker, Review of electronic transport models for thermoelectric materials, Superlatt. Microst. 44 (1) (2008) 1.
[40] A. Bulusu, D.G. Walker, Quantum modeling of thermoelectric performance of strained Si/Ge/Si superlattices using the nonequilibrium greens function method, J. Appl. Phys. 102 (7) (2007) 073713.
[41] T. Musho, D.G. Walker, Scalability of quantum simulations of thermoelectric superlattice devices, Comp. Mater. Sci. 50 (11) (2011) 3265–3269.
[42] T. Musho, D.G. Walker, Quantum simulation of nanocrystalline composite thermoelectric properties, Nanosc. Microsc. Therm. 16 (4) (2012) 288.
[43] A. Bulusu, D.G. Walker, Effect of quantum confinement on the thermoelectric properties of semiconductor 2d thin films and 1d wires, in: Thermal and Thermomechanical Proceedings 10th Intersociety Conference on Phenomena in Electronics Systems, 2006. ITHERM 2006., IEEE, 2006, p. 1299.
[44] A. Bulusu, D.G. Walker, Modeling of electron transport in thin films with quantum and scattering effects, in: ASME 2005 Pacific Rim Technical Conference and Exhibition on Integration and Packaging of MEMS, NEMS, and Electronic Systems collocated with the ASME 2005 Heat Transfer Summer Conference, American Society of Mechanical Engineers, 2005, p. 1427.
[45] M. Thesberg, M. Pourfath, N. Neophytou, H. Kosina, A non-equilibrium green functions study of energy-filtering thermoelectrics including scattering, International Conference on Large-Scale Scientific Computing, Springer, 2015, p. 301.
[46] M. Thesberg, M. Pourfath, H. Kosina, N. Neophytou, Thermoelectric power factor optimization in nanocomposites by energy filtering using negf, in: Proceedings of the 2015 International Workshop on Computational Electronics IWCE.
[47] R. Kim, M.S. Lundstrom, Computational study of the seebeck coefficient of one-dimensional composite nano-structures, J. Appl. Phys. 110 (3) (2011) 034511.
[48] R. Kim, M.S. Lundstrom, Computational study of energy filtering effects in one-dimensional composite nano-structures, J. Appl. Phys. 111 (2) (2012) 024508.
[49] V.K. Lamba, R.S. Sawhney, D. Engles, A.B. Garg, R. Mittal, R. Mukhopadhyay, Treatment of scattering in nano-films, in: AIP Conference Proceedings-American Institute of Physics, vol. 1349, 2011, p. 671.
[50] S. Wang, N. Mingo, Tailoring interface roughness and superlattice period length in electron-filtering thermoelectric materials, Phys. Rev. B 79 (2009) 115316.
[51] H. Li, Y. Yu, G. Li, Computational modeling and analysis of thermoelectric properties of nanoporous silicon, J. Appl. Phys. 115 (12) (2014) 124316.
[52] J. Li, T.C.A. Yeung, C.H. Kam, Influence of electron scatterings on thermoelectric effect, J. Appl. Phys. 112 (3) (2012) 034306.
[53] S. Cauley, M. Luisier, V. Balakrishnan, G. Klimeck, C.-K. Koh, Distributed non-equilibrium greens function algorithms for the simulation of nanoelectronic devices with scattering, J. Appl. Phys. 110 (4) (2011) 043713.
[54] S. Birner, T. Zibold, T. Andlauer, T. Kubis, M. Sabathil, A. Trellakis, P. Vogl, Nextnano: general purpose 3-D simulations, IEEE T. Electron Dev. 54 (9) (2007) 2137.
[55] Y.-M. Niquet, V.-H. Nguyen, F. Triozon, I. Duchemin, O. Nier, D. Rideau, Quantum calculations of the carrier mobility: methodology, Matthiessen's rule, and comparison with semi-classical approaches, J. Appl. Phys. 115 (5) (2014) 054512.
[56] J.E. Fonseca, T. Kubis, M. Povolotskyi, B. Novakovic, A. Ajoy, G. Hegde, H. Ilatikhameneh, Z. Jiang, P. Sengupta, Y. Tan, et al., Efficient and realistic device modeling from atomic detail to the nanoscale, J. Comput. Electron. 12 (4) (2013) 592.
[57] A.V. Kalitsov, M.G. Chshiev, J.P. Velev, Nonequilibrium coherent potential approximation for electron transport, Phys. Rev. B 85 (2012) 235111.
[58] M. Filoche, M. Piccardo, Y.-R. Wu, C.-K. Li, C. Weisbuch, S. Mayboroda, Localization landscape theory of disorder in semiconductors. I. Theory and modeling, Phys. Rev. B 95 (2017) 144204.
[59] A. Wacker, A.-P. Jauho, Quantum transport: the link between standard approaches in superlattices, Phys. Rev. Lett. 80 (1998) 369.
[60] A. Wacker, A.-P. Jauho, S. Rott, A. Markus, P. Binder, G.H. Döhler, Hot electrons in superlattices: quantum transport versus boltzmann equation, Physica B 272 (1) (1999) 157.
[61] A. Wacker, A.-P. Jauho, S. Rott, A. Markus, P. Binder, G.H. Döhler, Inelastic quantum transport in superlattices: success and failure of the boltzmann equation, Phys. Rev. Lett. 83 (4) (1999) 836.
[62] E. Flage-Larsen, Ø. Prytz, The Lorenz function: its properties at optimum thermoelectric figure-of-merit, Appl. Phys. Lett. 99 (20) (2011) 202108.
[63] H.-S. Kim, Z.M. Gibbs, Y. Tang, H. Wang, G.J. Snyder, Characterization of Lorenz number with Seebeck coefficient measurement, APL Mater. 3 (4) (2015) 041506.
[64] S. Datta, Electronic transport in mesoscopic systems, Cambridge Studies in Semiconductor Physics, Cambridge University Press, 1997.
[65] M. Buttiker, Coherent and sequential tunneling in series barriers, IBM J. Res. Dev. 32 (1) (1988) 63.
[66] C. Jacoboni, Theory of Electron Transport in Semiconductors: A Pathway from

Elementary Physics to Nonequilibrium Green Functions, Springer Series in Solid-State Sciences, Springer, Berlin, Heidelberg, 2010.
[67] C.W. Groth, M. Wimmer, A.R. Akhmerov, X. Waintal, Kwant: a software package for quantum transport, New J. Phys. 16 (6) (2014) 063065.
[68] http://kwant-project.org/.
[69] L. Musland, E. Flage-Larsen, Thermoelectric transport calculations using the Landauer approach, ballistic quantum transport simulations, and the Buttiker approximation, Comput. Mater. Sci. 132 (2017) 146–157.
[70] C. Jeong, R. Kim, M. Luisier, S. Datta, M. Lundstrom, On Landauer versus Boltzmann and full band versus effective mass evaluation of thermoelectric transport coefficients, J. Appl. Phys. 107 (2) (2010) 023707.
[71] U. Sivan, Y. Imry, Multichannel Landauer formula for thermoelectric transport with application to thermopower near the mobility edge, Phys. Rev. B 33 (1986) 551.
[72] R.L. Kronig, W.G. Penney, Quantum mechanics of electrons in crystal lattices, in: Proceedings of the Royal Society of London A: Mathematical, Physical and Engineering Sciences, Vol. 130, The Royal Society, 1931, pp. 499–513.
[73] M. Lundstrom, Fundamentals of Carrier Transport, 2nd ed., Cambridge University Press, 2000.
[74] E. Flage-Larsen, T4ME – Transport Properties for Materials: The Boltzmann Transport Equation for electrons in the relaxation time approximation. < https://espenfl.github.io/t4me > , 2017 (in preparation).